applied sciences

MDPI

Article

Study of the Dependence of Solar Radiation Regarding Design Variables in Photovoltaic Solar Installations with Optimal Dual-Axis Tracking

Francisco Javier Gómez-Uceda [1], Isabel Maria Moreno-Garcia [2,*], Álvaro Perez-Castañeda [3] and Luis Manuel Fernández-Ahumada [4]

[1] Department of Mechanics Engineering, Universidad de Córdoba, 14071 Cordoba, Spain; fjgomez@uco.es
[2] Department of Electronic and Computer Engineering, Universidad de Córdoba, 14071 Cordoba, Spain
[3] Physics for Renewable Energies Research Group, Universidad de Córdoba, 14071 Cordoba, Spain; perezcastanedaalvaro@gmail.com
[4] Department of Electrical Engineering and Automatics, Universidad de Córdoba, 14071 Cordoba, Spain; lmfernandez@uco.es
* Correspondence: isabel.moreno@uco.es; Tel.: +34-9572-12533

Abstract: Solar tracking is an efficient strategy to increase the radiative capture of photovoltaic collectors. Within the multiple efforts made in recent decades to improve the production of these facilities, various works have studied solutions to optimize the number of rotation axes (single or dual rotation axes), the degree of collector coverage, the distances between trackers, the geometric arrangement of trackers or the minimization of shading between collectors. However, although in this type of installation it is common to find collectors with geometric shapes other than rectangles, no studies on the influence of the shape of the collectors on the radiative incidence are found in the literature. In this connection, the present work systematically addresses the study of incident solar radiation in photovoltaic installations with dual-axis trackers with collectors of different geometric shapes. By means of the exhaustive study, the conclusion is drawn that, for dual-axis photovoltaic installations with an optimal tracking strategy, the main variables that influence the annual radiative incidence are the spacing between collectors, the coverage ratio (GCR), and the collector surface, while the type of arrangement of collectors and the shape of these do not show predictive values.

Keywords: photovoltaics; dual-axis solar trackers; shading in PV plants; solar tracking; backtracking

Citation: Gómez-Uceda, F.J.; Moreno-Garcia, I.M.; Perez-Castañeda, A.; Fernández-Ahumada, L.M. Study of the Dependence of Solar Radiation Regarding Design Variables in Photovoltaic Solar Installations with Optimal Dual-Axis Tracking. *Appl. Sci.* **2021**, *11*, 3917. https://doi.org/10.3390/app11093917

Academic Editors: Giovanni Petrone and Richard Yong Qing Fu

Received: 18 March 2021
Accepted: 23 April 2021
Published: 26 April 2021

1. Introduction

There is no doubt about the important role that energy plays in our societies. Its implications go beyond mere technical aspects. Social structuring, economic development, and the environment, among others, are aspects that make up the complex implication of energy in the global agenda [1]. In this context, renewable energies have been experiencing sustained growth in recent years. Thus, the International Energy Agency (IEA) foresees a record increase of 218 GW in the year 2021 in the net capacity of renewable electricity installed in the world, in an average scenario, that could reach up to 266 GW, in an accelerated scenario [2]. In fact, during the first quarter of 2020, renewable energies were the only source of electricity whose demand increased despite the 2.5% decrease in global electricity demand caused by the blockades implemented by different governments to curb the spread of COVID-19 [3].

Within the field of renewables, solar energy, in general, and photovoltaic (PV), in particular, are candidates to satisfy a large part of the global energy demand in the coming years due to their abundance and competitiveness [4]. In fact, in the IEA predictions for

the year 2021, solar PV accounts for 54% of the growth in the world's installed net renewable electricity capacity [2]. The remarkable progress that the technology associated with the implementation of photovoltaic energy has been experiencing has not only driven its boom in recent years [5,6] but this growth is expected to accelerate during the 2023–25 period [2].

One of the fundamental factors in the energy production of PV plants is the incident solar irradiance on the collectors. Among the various strategies that exist to increase this irradiance in solar collectors and, therefore, energy production in PV plants, is solar tracking, which is a technological niche in which there are still possible improvements that can contribute to such an increase [5]. This strategy is in contrast with fixed panel structures that have a constant orientation towards the sun depending on the latitude of the place where the PV installation is located. Thus, in the case of solar trackers, the PV modules move while looking for an orientation that generates more energy, either by capturing solar energy for as long as possible [7] or by capturing maximum solar irradiance [8,9].

The most common classification of trackers is established based on the number of axes used to move the modules. Thus, we speak of tracking systems on one axis (movement in azimuth or elevation) or on two axes (movement in azimuth and elevation). Improving the technology of solar tracking systems is an important objective considering the high demand of energy resources, being the research niche for many authors. For example, in [7], different tracker motion control systems are studied with regard to their economic evaluation. In [8], the different solar trackers are studied in depth, performing a comparison between them in terms of efficiency, performance, advantages, and disadvantages, while other studies perform an in-depth review of the related literature to define the advantages of the applicability of solar tracking [10,11].

In the scientific literature, there are studies that question the use of trackers with one or two axes versus fixed systems or one axis versus two. Specifically, various studies are being developed that question the various possibilities that arise in terms of efficiency, cost, location, production, etc., which is a real scientific challenge. For example, in [12–14], authors analyze the effect of different solar trackers strategies considering the location. Other authors provide profits of the tracking photovoltaic systems in comparison with fixed photovoltaic systems [15,16]. An interesting result is the one presented in [17], where a method for optimal storage capacity was calculated under the power-curtailment and storage/discharge requirements. Hence, although solar tracking systems have a higher cost than fixed systems, their maintenance is more complex and their exposure to environmental conditions is greater [18]; the performance of dual-axis trackers are greater than those of fixed systems [19,20] and single-axis trackers [21–23]. Bahrami states in [21] that a dual-axis tracking system would result in greater irradiance than a single-axis due to its ability to minimize losses associated with cosine effect. Authors in [22] highlight their conclusion that using the two-axis sun tracker system enables the PV panel to collect and produce higher amounts of electrical energy than using single-axis and fixed structures; their study considered five configurations of sun tracking systems and two traditional fixed panels. The results presented in [23] show that the optimal trajectories for the tilt and azimuth angle depend on the available solar radiation, solar cell efficiency, tracking system consumption, and the optimization bounds. Therefore, based on these studies, it can be affirmed that the choice of the type of strategy depends on several factors, it being necessary to delve into the technological and economic components to reach useful conclusions [5].

Regarding the tracking mechanism, different driver methods can be distinguished to achieve the objectives of the collector movement [8]. Among them, the sensor driver systems stand out, whose operation is based on the variation of light received by optical sensors that cause the movement of the collectors looking for the position of the sun. Additionally, there are microprocessor driver systems that incorporate small processors with movement strategies programmed through mathematical models to locate the position of the sun. Within these in the bibliography are the open-loop driver systems that modify

the movement of the actuators of the modules from mathematical equations that fix the position of the sun from the day and the hour. In contrast, closed-loop driver systems modify the movement of the actuators based on the information provided by position sensors, recalculating the position of the sun. Finally, intelligent driver systems incorporate artificial intelligence techniques to control the movement of collectors [24].

Another of the determining factors in the performance of a PV plant is the shading of its modules, since these shadows not only imply a lower incident irradiance [25] but also give rise to the appearance of hot spots that bring with them overheating and losses in energy production [26]. In this regard, the behavior of PV modules when they are partially shaded has been widely debated. Several simulation models have been used to find a configuration less susceptible to shadow problems of solar cells [27–30]. Specifically, Díaz-Dorado et al. [31] have analyzed the effect of shading in a PV tracker with partially shaded astronomical tracking based on the exact arrangement of shaded cells and modules. Other authors have analyzed the energy cost in the production of PV plants as a function of the connections between the cells and the modules [32] of the ground cover ratio (GCR) of the plant that depends on the variables of their design [33] or of the tracking strategy [26,34].

One possible solution to alleviate the effect of shadows in PV plants with solar tracking is back tracking [35], which consists of modifying the orientation of the collecting surfaces in shading situations between panels in order to eliminate such shadows. Another possible solution is to modify the geometry of the collecting surfaces. Thus, although most of the PV panels found in PV plants connected to grids are rectangular, there are already some installations with dual-axis solar tracking where the collectors have other geometric shapes, such as those developed by the Deger Ibérica company in Tarragona (Spain), Ontario (Canada), or Estonia, with 15.6 kWp, 24 MWp, and 100 kWp installed, respectively [36]. However, no previous works have been found in the literature aimed at characterizing the geometric shape of the collectors or their degree of modularity in terms of optimizing the performance of a photovoltaic installation in the event of the possible incidence of shading.

In this context, in the present work, the annual radiative uptake has been quantified in a wide set of PV installations with dual-axis monitoring with different geometries in which the shape of the collectors and the design parameters have been systematically varied. For each case, it has been assumed that the collectors follow the optimal solar tracking strategy proposed by Fernández-Ahumada et al. [37,38]. Unlike traditional solar tracking methods that search for the position of the sun at each moment using astronomical models [39–41], according to this strategy, the collecting planes are oriented at each instant of time towards the direction of space in which the irradiance is maximum, except during the moments when such orientation implies the shading of one collector over another. When this occurs, normally at the beginning and end of the day, the collectors are oriented in the direction in which, without causing shading, the incident irradiance on the collectors is maximum. In this way, the production of each installation, which is considered proportional to annual solar radiation, is calculated under the hypothesis that each installation will follow an optimal tracking strategy adapted to its own geometry. Therefore, this study aims to advance the characterization of the electrical behavior of shaded solar trackers, which is an issue where the scientific community has made a considerable effort, simulating tracking strategies for an improvement in photovoltaic production [12,14,42].

To achieve this objective, after this introduction in which the scientific advances made by the scientific community in the field of solar tracking in PV plants are presented, the following section describes the methodology followed in this study to simulate annual solar radiation incident on collectors with a dual-axis tracking strategy that optimizes radiative uptake while avoiding shading between collectors. Similarly, the methodology established for the study of the influence of the design parameters of a PV plant on this annual solar irradiance is explained. Based on this, Section 3 presents the results when applying the methodology described to an existing PV plant ("El Molino", Córdoba,

Spain) with its design parameters systematically modified. Similarly, an adjustment model is proposed that represents in a simplified manner the dependence of the annual solar irradiance with respect to the design variables studied, and these dependencies are quantified. Finally, in Section 4, the main conclusions of the present study are presented.

2. Methodology

2.1. Vector Treatment of the Solar Position and the Estimation of the Solar Irradiance in the Celestial Sphere

In accordance with the above, this work presents a study of the influence of design variables on the performance of a PV plant with dual-axis tracking and optimal tracking strategy. This tracking strategy, which is described in the following section, will determine the orientation of the solar collectors at all times, which allows for optimizing radiative capture while avoiding shadows between collectors. In the present work, to determine at each instant of time the orientation of these collectors, as well as the position of the Sun in the celestial sphere, vector notation is used.

Figure 1 shows the coordinate system used, with the Ox axis oriented towards the west, the Oy axis towards the south, and the Oz axis towards the zenith. In this equation, $\vec{\imath}$, $\vec{\jmath}$, and $\vec{k}$ are the unit vectors on the axes Ox, Oy, and Oz, respectively; the unit vector that points towards the Sun, called the solar vector, $\vec{s}$, will be expressed by Equation (1), in which φ is the latitude of the place, δ the declination, and t the solar hour.

$$\vec{s} = s_x\vec{\imath} + s_y\vec{\jmath} + s_z\vec{k} = sin\Omega t cos\delta\vec{\imath} + (cos\Omega t cos\delta sin\varphi - sin\delta cos\varphi)\vec{\jmath} + (cos\Omega t cos\delta cos\varphi + sin\delta sin\varphi)\vec{k} \quad (1)$$

Equation (2) shows the mathematical expression proposed by Spencer (1971) for calculating the declination, δ, as a function of the daily angle, Γ, which in turn depends on the Julian day, d_n, according to Equation (3).

$$\delta(rad) = 0.006918 - 0.399912\,cos(\Gamma) + 0.070257 sin(\Gamma) - 0.006758\,cos(2\Gamma) + 0.000907 sin(2\Gamma) - 0.002697\,cos(3\Gamma) + 0.00148 sin(3\Gamma) \quad (2)$$

$$\Gamma(rad) = \frac{2\pi(d_n - 1)}{365} \quad (3)$$

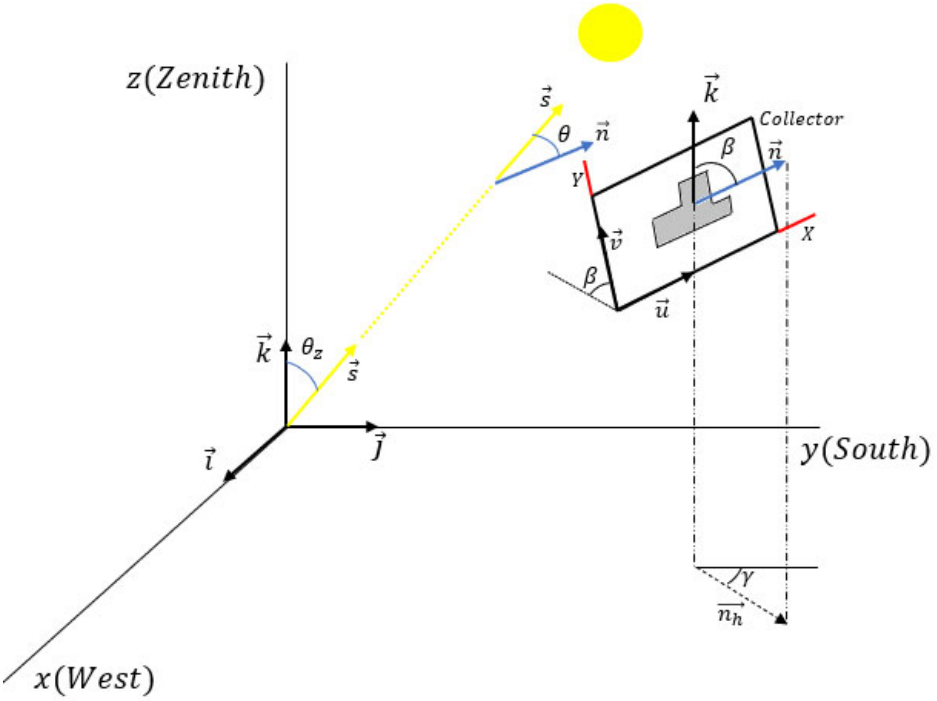

Figure 1. Astronomical and geometric magnitudes considered.

The orientation of the collector plane at each instant of time can be represented by the unit vector perpendicular to it, $\vec{n}$, or by the pair of unit vectors, $\vec{u}$ and $\vec{v}$, contained in the collector plane, of which $\vec{u}$ is horizontal and $\vec{v}$ is parallel to the maximum slope direction of the collector plane (Figure 1). Thus, γ and β being the angles representing the azimuth and inclination of the collectors, respectively, the vectors $\vec{n}$, $\vec{u}$, and $\vec{v}$ will be given by Equations (4)–(6), respectively.

$$\vec{n} = sin\beta\ sin\gamma\vec{\imath} + sin\beta cos\gamma\vec{\jmath} + cos\beta\vec{k} \quad (4)$$

$$\vec{u} = -cos\gamma\ \vec{\imath} + sin\gamma\vec{\jmath} \quad (5)$$

$$\vec{v} = -cos\beta\ sin\gamma\vec{\imath} - cos\beta cos\gamma\vec{\jmath} + sin\beta\vec{k} \quad (6)$$

For the characterization of the incident solar irradiance on the collector planes, the model of Perez et al. [43] has been used. According to this model, the global solar irradiance, I, on an inclined plane at an angle β is the sum of the direct, diffuse, and reflected irradiance on an inclined plane, which, in turn, depends on the direct irradiance, I_B, and diffuse, I_D, on a horizontal surface, according to Equation (7), where θ is the angle between the normal vector and the collector plane $(\vec{n})$ and the solar vector $(\vec{s})$, θ_z is the zenith angle, ρ is the albedo of the surface of incidence of the irradiance before being reflected towards the collector, a and b are parameters given by Equations (8) and (9), and F_1 and F_2 are the weighting factors for the decomposition of the inclined diffuse radiation, the second addition, in the three subcomponents considered by the authors: isotropic diffuse, circumsolar diffuse, and diffuse from the horizon (Perez et al., 1990).

$$I = \frac{cos\,\theta}{cos\,\theta_z} I_B + \left[(1 - F_1)\frac{1 + cos\,\beta}{2} + F_1\frac{a}{b} + F_2\,sin\,\beta\right] I_D + \rho\frac{1 - cos\,\beta}{2}(I_B + I_D) \quad (7)$$

$$a = \max(\cos\theta, 0) \quad (8)$$

$$b = \max(\cos 85°, \cos\theta_z) \quad (9)$$

Substituting the vector expressions (10), (11), and (12) in Equation (7), we obtain Equation (13), in which the dependence of I on $\vec{n}$ is made explicit,

$$cos\,\beta = \vec{k} \cdot \vec{n} \tag{10}$$

$$cos\,\theta = \vec{s} \cdot \vec{n} \tag{11}$$

$$cos\,\theta_z = \vec{s} \cdot \vec{k} \tag{12}$$

$$I = \frac{\vec{s} \cdot \vec{n}}{\vec{s} \cdot \vec{k}} I_B + \left[(1 - F_1) \frac{1 + \vec{k} \cdot \vec{n}}{2} + F_1 \frac{\vec{s} \cdot \vec{n}}{b} + F_2 \sqrt{1 - \left(\vec{k} \cdot \vec{n}\right)^2} \right] I_D + \rho \frac{1 - \vec{k} \cdot \vec{n}}{2} (I_B + I_D) \tag{13}$$

The production of a PV plant will be greater to the extent that the incident irradiance on its collectors is greater. In this regard, Fernández-Ahumada et al. [37] showed that the incident irradiance on the collectors is maximum when they are oriented in such a way that their normal vector verifies Equation (14). In accordance with this result, the authors propose a new tracking strategy for PV plants with dual-axis trackers in which they are oriented according to Equation (14), and consequently, radio capture and energy production are optimized.

$$\vec{n} = \frac{\frac{\partial I}{\partial (\vec{s} \cdot \vec{n})} \vec{s} + \frac{\partial I}{\partial (\vec{k} \cdot \vec{n})} \vec{k}}{\sqrt{\left(\frac{\partial I}{\partial (\vec{s} \cdot \vec{n})}\right)^2 + \left(\frac{\partial I}{\partial (\vec{k} \cdot \vec{n})}\right)^2 + 2 \left(\frac{\partial I}{\partial (\vec{s} \cdot \vec{n})}\right) \left(\frac{\partial I}{\partial (\vec{k} \cdot \vec{n})}\right) \vec{s} \cdot \vec{k}}} \tag{14}$$

Therefore, when applying this tracking strategy to the model of Perez et al. (1990), the partial derivatives given by expressions (15) and (16) are obtained. Substituting these results in Equation (14), Equation (17) is obtained, which represents the direction of the normal vector to the collecting planes corresponding to the optimal tracking strategy proposed by Fernández-Ahumada et al. [37] for PV plants with dual-axis tracking.

$$\vec{n} = \frac{\frac{\partial I}{\partial (\vec{s} \cdot \vec{n})} \vec{s} + \frac{\partial I}{\partial (\vec{k} \cdot \vec{n})} \vec{k}}{\sqrt{\left(\frac{\partial I}{\partial (\vec{s} \cdot \vec{n})}\right)^2 + \left(\frac{\partial I}{\partial (\vec{k} \cdot \vec{n})}\right)^2 + 2 \left(\frac{\partial I}{\partial (\vec{s} \cdot \vec{n})}\right) \left(\frac{\partial I}{\partial (\vec{k} \cdot \vec{n})}\right) \vec{s} \cdot \vec{k}}} \tag{15}$$

$$\frac{\partial I}{\partial (\vec{k} \cdot \vec{n})} = \left(\frac{(1 - F_1)}{2} - F_2 \frac{\vec{k} \cdot \vec{n}}{\sqrt{1 - \left(\vec{k} \cdot \vec{n}\right)^2}} \right) I_D - \rho \frac{(I_B + I_D)}{2} \tag{16}$$

$$\vec{n} = \frac{\left(\frac{I_B}{\vec{s} \cdot \vec{k}} + F_1 \frac{I_D}{b}\right) \vec{s} + \left(\frac{(1 - F_1)\, I_D}{2} - F_2 \frac{\vec{k} \cdot \vec{n}}{\sqrt{1 - \left(\vec{k} \cdot \vec{n}\right)^2}} I_D - \rho \frac{(I_B + I_D)}{2} \right) \vec{k}}{\sqrt{\left(\frac{I_B}{\vec{s} \cdot \vec{k}} + F_1 \frac{I_D}{b}\right)^2 + \left(\frac{(1 - F_1)\, I_D}{2} - F_2 \frac{\vec{k} \cdot \vec{n}}{\sqrt{1 - \left(\vec{k} \cdot \vec{n}\right)^2}} I_D - \rho \frac{(I_B + I_D)}{2} \right)^2 + 2 \left(\frac{I_B}{\vec{s} \cdot \vec{k}} + F_1 \frac{I_D}{b}\right) \left(\frac{(1 - F_1)\, I_D}{2} - F_2 \frac{\vec{k} \cdot \vec{n}}{\sqrt{1 - \left(\vec{k} \cdot \vec{n}\right)^2}} I_D - \rho \frac{(I_B + I_D)}{2} \right) \vec{s} \cdot \vec{k}}} \tag{17}$$

Given the difficulty of solving the variable $\vec{n}$ in Equation (17), an iterative method based on the series convergence of vectors $\{\vec{n}_0 (= \vec{s}), \vec{n}_1, \vec{n}_2, \ldots, \vec{n}_j\}$ is proposed, in which each vector $\vec{n}_j$ is obtained as a function of $\vec{n}_{j-1}$ according to Equation (18), and consequently, $\vec{n}$ will be given by Equation (19). Given the nature of the problem, in this work, it has been considered that $j = 25$ is a sufficiently high value since the correct convergence of this value has been verified for all the practical cases studied.

ç

$$\vec{n}_j = \frac{\left(\frac{I_B}{\vec{s}\cdot\vec{k}} + F_1\frac{I_D}{b}\right)\vec{s} + \left(\frac{(1-F_1)\,I_D}{2} - F_2\frac{\vec{k}\cdot\vec{n}_{j-1}}{\sqrt{1-\left(\vec{k}\cdot\vec{n}_{j-1}\right)^2}}I_D - \rho\frac{(I_B+I_D)}{2}\right)\vec{k}}{\sqrt{\left(\frac{I_B}{\vec{s}\cdot\vec{k}} + F_1\frac{I_D}{b}\right)^2 + \left(\frac{(1-F_1)\,I_D}{2} - F_2\frac{\vec{k}\cdot\vec{n}}{\sqrt{1-\left(\vec{k}\cdot\vec{n}\right)^2}}I_D - \rho\frac{(I_B+I_D)}{2}\right)^2 + 2\left(\frac{I_B}{\vec{s}\cdot\vec{k}} + F_1\frac{I_D}{b}\right)\left(\frac{(1-F_1)\,I_D}{2} - F_2\frac{\vec{k}\cdot\vec{n}}{\sqrt{1-\left(\vec{k}\cdot\vec{n}\right)^2}}I_D - \rho\frac{(I_B+I_D)}{2}\right)\vec{s}\cdot\vec{k}}} \quad (18)$$

$$\vec{n} = \lim_{j\to\infty}\vec{n}_j \quad (19)$$

2.2. Method to Avoid Inter-Shading of Collectors

According to the studies found in the bibliographic review, the shading of solar panels negatively affects their energy production. Therefore, to optimize the performance of a PV plant with dual-axis solar trackers, as those discussed in this study, it is necessary to accompany an adequate tracking strategy with a procedure that prevents the collectors from shading each other.

In this regard, Fernández-Ahumada et al. [38] presented a dichotomous criterion to quickly determine whether or not there is inter-shading between collectors. The method is based on the fact that, in an installation with collectors of the same geometric shape oriented towards the same direction of the celestial sphere (characterized by its normal vector, $\vec{n}$), the shadow cast by a collector Π_i on the plane ψ that contains the reference collector Π_0 is a polygon Π'_i with the same shape as the contour of the collector (Figure 2).

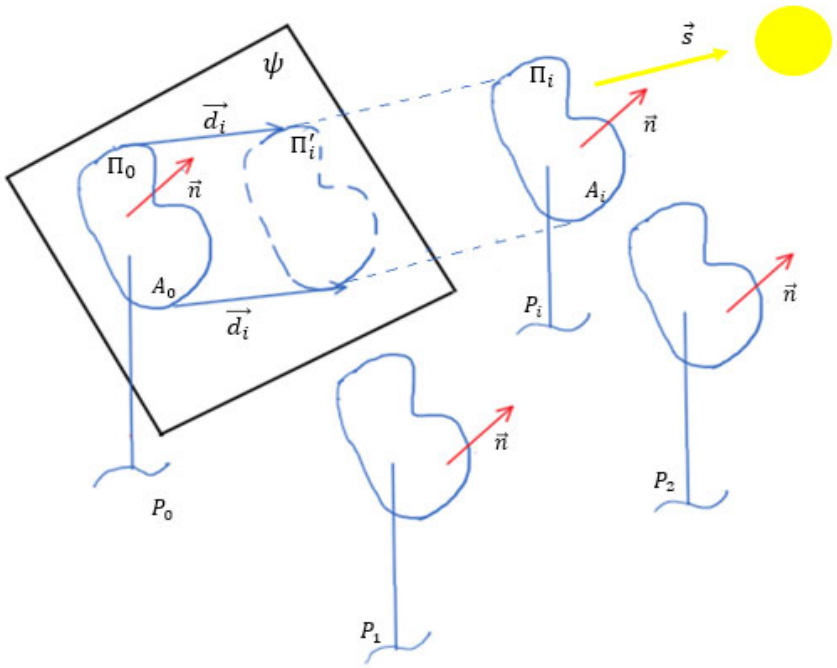

Figure 2. Astronomical and geometric magnitudes considered.

Hence, vector $\vec{d}_i$ is the geometric displacement vector from polygon Π_0 to Π'_i. This vector, as shown by the authors, is obtained through the Equation (20), although it must

be considered that, for the collector Π_i to be able to shade the collector Π_0, the conditions expressed in Equations (21)–(23) must be fulfilled.

$$\vec{d}_i = \overrightarrow{P_oP_i} - \frac{\overrightarrow{P_oP_i}\cdot\vec{n}}{\vec{s}\cdot\vec{n}}\vec{s} \quad (20)$$

$$\vec{s}\cdot\vec{k} > 0 \quad (21)$$

$$\vec{s}\cdot\vec{n} > 0 \quad (22)$$

$$\overrightarrow{P_0P_i}\cdot\vec{n} > 0 \quad (23)$$

From expression (20), given that $\vec{d}_i$ is a vector included in the collector plane ψ, Equations (24) and (25) allow for determination of the components of this vector in the OXY reference system contained in the plane ψ and defined by the vectors $\vec{u}$ y $\vec{v}$.

$$d_{Xi} = \vec{d}_i \cdot \vec{u} \quad (24)$$

$$d_{Yi} = \vec{d}_i \cdot \vec{v} \quad (25)$$

Knowing $\vec{d}_i$ and its components d_{Xi} and d_{Yi}, the dichotomous criterion proposed by Fernández-Ahumada et al. [38], based on Minkowski's algebra [44–46] and whose validity is demonstrated in Appendix A, it is established that there will be an intersection of the polygons Π_0 and Π'_i. Therefore, mutual shading between the panels Π_0 y Π_i, if, when representing vector $\vec{d}_i$ from the origin of coordinates, the end of the vector is included within the plane curve Σ, which is obtained as the envelope of the family of all polygons that can be drawn on the plane ψ by translating the polygon Π_0 with the condition that its perimeter is in contact with the coordinate origin of the reference system contained in ψ (Figure 3).

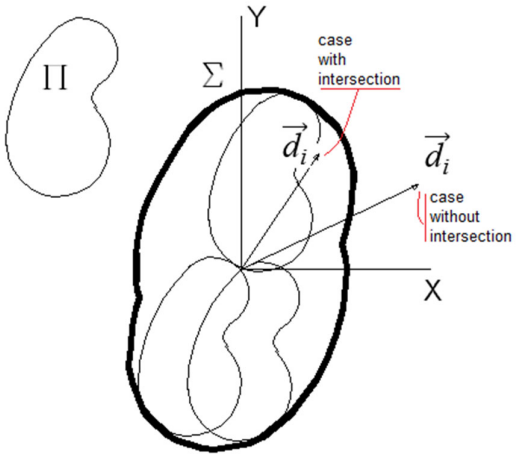

Figure 3. Determination of Σ, auxiliary curve of the intersection criterion and existence of shadow between panels.

It is important to note that, since photovoltaic collectors are built by annexing rectangular photovoltaic modules, the resulting geometric shape for the collector is, in general, a closed polygon in which all sides of the perimeter are contained in two directions perpendicular to each other, as shown by the orange line in Figure 4. This fact leads to the determination of the envelope Σ being simplified and able to be performed analytically. Furthermore, this envelope (blue trace in Figure 4) will also be a closed polygon with the

sides parallel and perpendicular to the directions of the perimeter of the collectors (Figure 4). Therefore, the envelope is mathematically described by the coordinates $X_{env}(k)$ and $Y_{env}(k)$ of each vertex k of the polygon ($1 < k < N_{env}$, N_{env} being the total number of vertices of Σ). In Appendix B, the analytical obtaining of the enclosure for photovoltaic collectors is detailed in a generic way.

According to Figure 4, the end of vector $\vec{d}_i$ would be located inside the envelope Σ and, therefore, there would be shading between the panels Π_0 y Π_i if there is some vertex k for which the mathematical condition given by Equation (26) is fulfilled.

$$\left[sign(d_{Xi}) = sign\left(X_{env}(k)\right)\right] and \left[sign(d_{Yi}) = sign\left(Y_{env}(k)\right)\right] and \\ \left[|d_{Xi}| < |X_{env}(k)|\right] and \left[|d_{Yi}| < |Y_{env}(k)|\right] \quad (26)$$

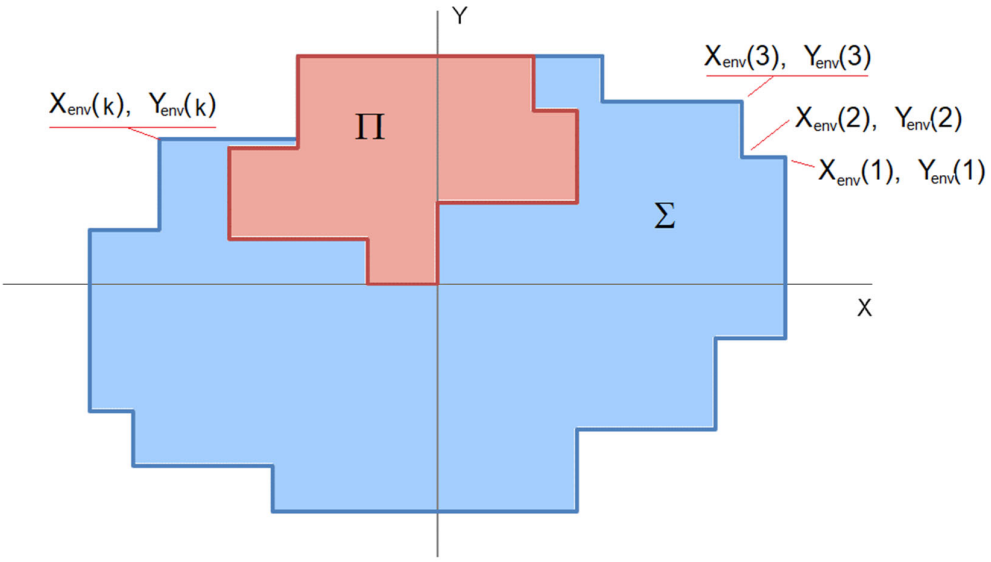

Figure 4. Form. Generic shape of a solar collector (orange) and its envelope Σ (blue).

In accordance with the above, Figure 5 shows, by means of a flow diagram, the inter-shading $(\vec{n})$ function, especially designed to implement the method described in this section to determine the existence of shadow between modules in PV installations with dual-axis tracking and regular distribution of collectors. This Boolean function depends on the vector $\vec{n}$, Equation (19), returning a value "true" if $\vec{n}$ implies inter-shading and "false" otherwise. As can be seen in Figure 5, only possible shading is studied in the reference collector, considered representative of the set, which is totally surrounded by N_t trackers.

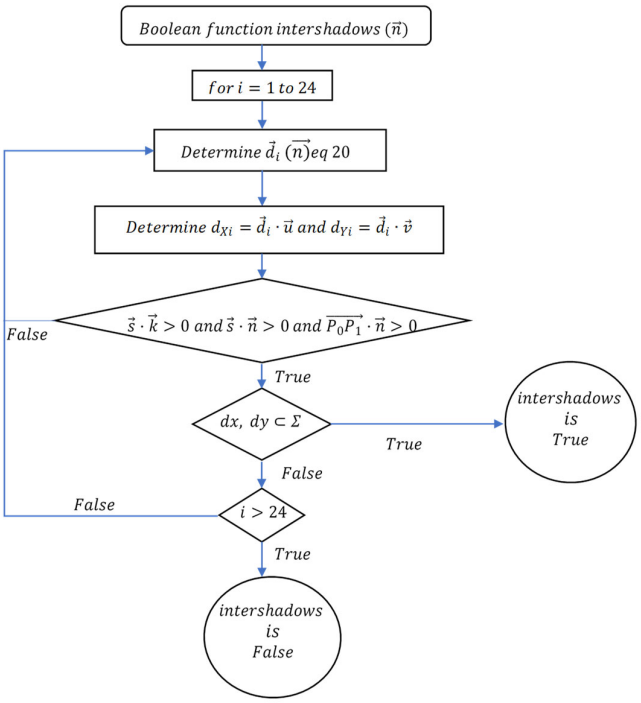

Figure 5. Flow diagram of the inter-shading function ($\vec{n}$).

In this way, in the case that the value of $\vec{n}$, obtained from Equation (19), does not imply shadows between collectors, $intershadows(\vec{n}) = False$, the optimal tracking strategy will propose the orientation of the collectors according to the address of $\vec{n}$. On the contrary, if the value of $\vec{n}$, obtained from Equation (19), implies shadows between collectors, $intershadows(\vec{n}) = True$, the orientation that does not imply shadows and that maximizes the incident irradiance must be sought. In that case, back tracking is used following the process indicated in Figure 6.

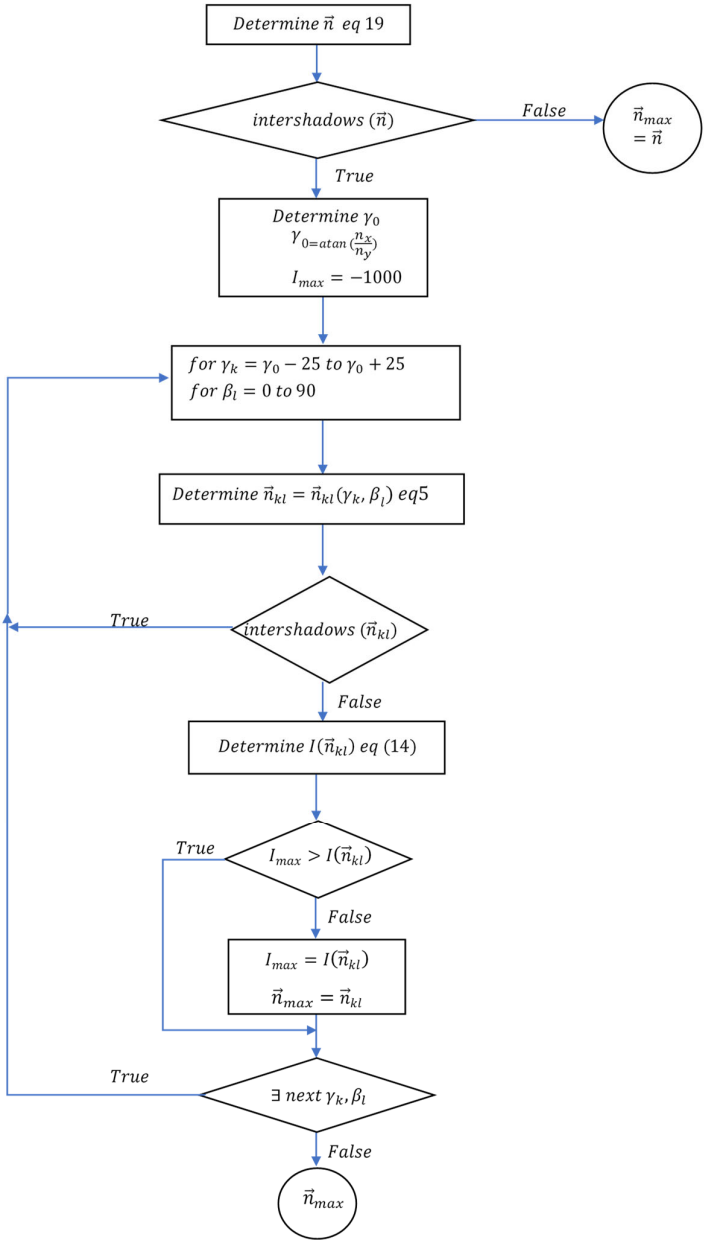

Figure 6. Flow diagram to determine the orientation $\vec{n}$ of maximum irradiance uptake without any inter-shading between collectors.

2.3. Calculation Scheme of Intercepted Solar Radiation

With the methodology described for solar tracking, the incident solar irradiance on solar collectors has been simulated for the 12 representative days, according to Klein [47]. From this irradiance, the incident radiation on the collectors on each representative day m has been calculated using Equation (27), where the integral has been approximated by discretizing the sum in time intervals of three minutes.

$$H_m = \int_{t_{sunrise,m}}^{t_{sunset,m}} \left[\frac{\vec{s}\cdot\vec{n}}{\vec{s}\cdot\vec{k}} I_B + \left[(1-F_1)\frac{1+\vec{k}\cdot\vec{n}}{2} + F_1\frac{\vec{s}\cdot\vec{n}}{b} + F_2\sqrt{1-\left(\vec{k}\cdot\vec{n}\right)^2} \right] I_D + \rho\frac{1-\vec{k}\cdot\vec{n}}{2}(I_B + I_D) \right] dt \quad (27)$$

Once the daily radiation has been calculated for the representative days proposed by Klein [47] for each of the 12 months of the year (m = 1,2, ..., 12), the annual global radiation

(H_{year}) is calculated according to Equation (28), where N_m is the number of days in the month m.

$$H_{year} = \sum_{m=1}^{12} N_m \cdot H_m \tag{28}$$

2.4. Cases Analyzed

In this work, the effect of the shape of the collectors on the capture of annual radiation in a PV plant with dual-axis tracking has been studied. To generate the study scenarios, the design of "El Molino", a photovoltaic installation located in Córdoba (latitude = 37.75492° N; longitude = 5.04548° W) was used as a starting point. It is an installation with dual-axis trackers (with azimuth and elevation movement) and rectangular collectors 8 m wide and 5 m high. Each collector is made up of 25 photovoltaic modules 1m high and 1.6m wide (Figure 7a). The trackers are arranged in a regular grid on horizontal ground, initially separated by a distance D_{EW} =20 m in the EW direction and D_{NS} =14 m in the NS direction (Figure 7b).

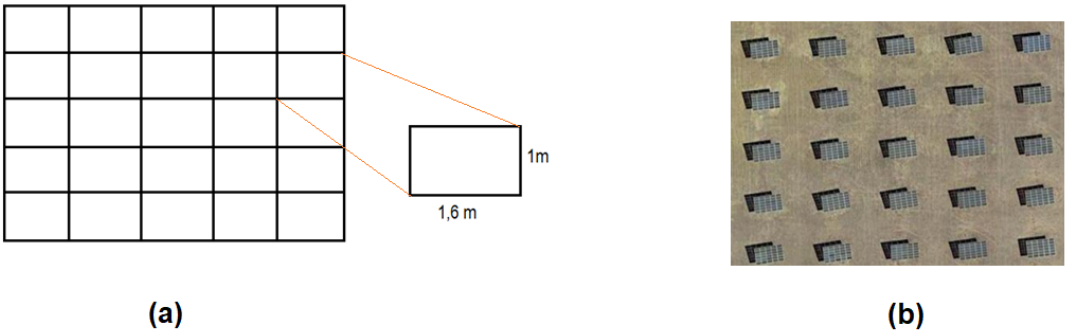

Figure 7. Design characteristics of the "El Molino" facility: (**a**) Constitution of the collectors; (**b**) Arrangement of collectors.

Case studies arise by introducing different variations in the original design and crossing all possible sources of variation. Specifically, the variations introduced consist of:

- *Modification of the collector shape*. The possibility of introducing cuts at the vertices has been considered to study the collectors with the shape indicated in Figure 8. Letting (X_{ul}, Y_{ul}), (X_{ur}, Y_{ur}), (X_{dl}, Y_{dl}), and (X_{dr}, Y_{dr}) be the coordinates of the vertices corresponding to the cuts made in the upper left, upper right, lower left, and lower right corners, the possible values considered (in metres) for each of these pairs were (0,0), (1,1.6), (1,3.2), (2,1.6), and (2,3.2). The crossing of all the possibilities generated N_G = 5^4 = 625 different forms of collector.
- *Modification of the inter-distances*. Letting D_{NS} be the distance in the NS direction between rows of collectors and D_{EW} the distance in the EW direction between columns of collectors, the possibilities D_{NS} = 10 m, 12.5 m, 15 m, 17.5 m, and 20 m and D_{EW} = 10 m, 15 m, 20 m, and 25 m were studied. The crossing of these possibilities gave rise to N_D = 20 designs of different distances.
- *Modification of the spatial distribution of the solar trackers.* For each pair of distances (D_{NS}, D_{EW}), N_S = 2, possible spatial distributions of the solar trackers in the plant were studied, both the regular grid arrangement oriented to the south (Figure 9a) and staggered (Figure 9b). In both configurations, it was considered that the reference collector in the study (i = 0) was surrounded by 24 collectors.

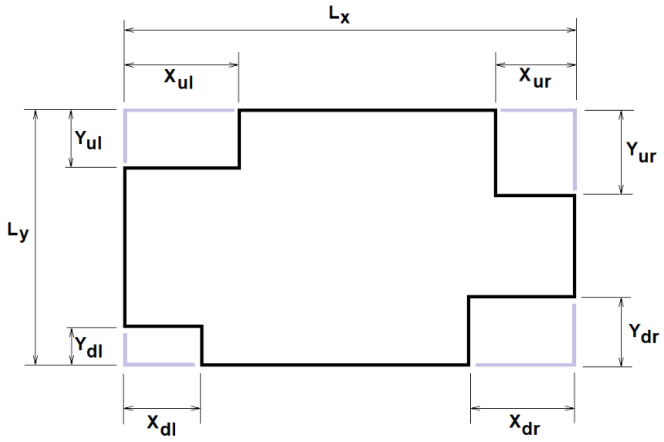

Figure 8. Generic way of describing the clipped vertex collector.

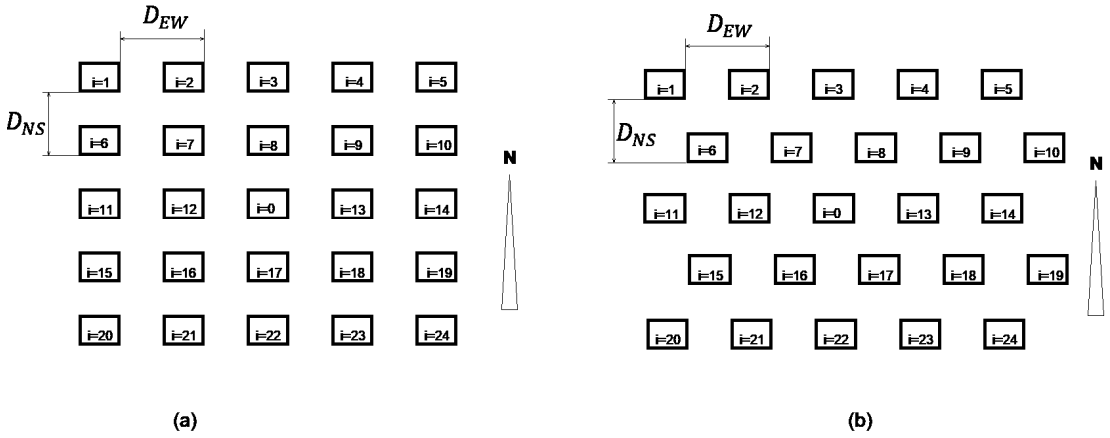

Figure 9. Considered spatial arrangements and location of the reference collector in the study (i = 0): (**a**) regular grid; (**b**) staggered.

The crossing of all the possibilities generated $N_T = N_G \cdot N_D \cdot N_S = 25000$ different combinations of geometric designs for the PV plant "El Molino" with dual-axis tracking and its collectors. For each of these designs, the annual incident radiation on the collectors was obtained by the method set forth, Equation (28), considering the 12 characteristic days proposed by Klein [47], and the monthly mean radiation values [48] set forth in Table 1.

Table 1. Data considered for the estimation of the annual solar irradiance in "El Molino" PV Plant (Cordoba, Spain): horizontal daily radiation, H [48] and representative day proposed by [47] each month of the year.

Month	H (J/m²)	Representative Day
January	7401000	17
February	11097000	47
March	14158000	75
April	17307000	105
May	19017000	135
June	24263000	162
July	25719000	198
August	23411000	228
September	17983000	258

October	11895000	288
November	8228000	318
December	6237000	344

3. Results

This section describes the incident radiation values on collectors and the results of the study of the influence of the design variables on the solar incidence on the PV plant designs considered. The synoptic values obtained for the annual incident radiation in collectors are summarized in Table 2. Figure 10 shows the distribution of values obtained depending on the membership intervals.

Table 2. Descriptive parameters of the set of values of H_{year} (kWh/m²).

Number of Cases	**25000**
Average	2172.0
Minimum	2040.2
Maximum	2233.8
Median	2189.6

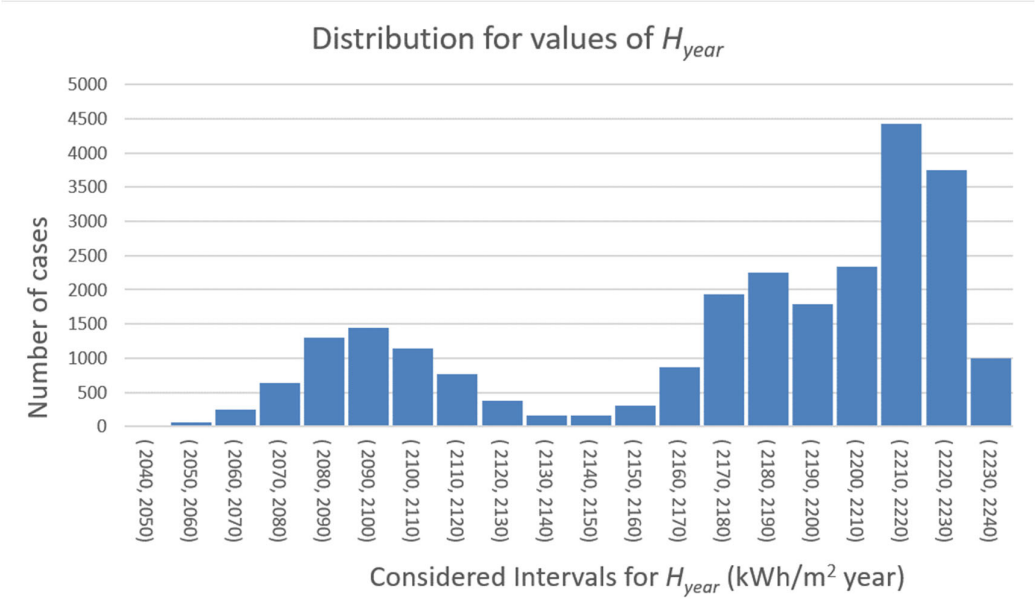

Figure 10. Distribution of annual solar radiation values (H) according to membership intervals.

In the set of values obtained, it is observed that certain forms of the collector offer the same value. These are the cases in which the set of cuts A, B, C and D of Figure 11a are permuted as shown in Figure 11b–d,f–i. A detailed analysis of the procedure followed makes it possible to verify that the shape of the solar collector does not influence directly but rather through its envelope. As a consequence, the collector shapes of the first column (11 (a), 11 (b), 11 (c), 11 (d)) give rise to identical annual radiation results since they all give rise to the same envelope Σ (represented in Figure 11e). On the other hand, the coincidence of radiation outcomes in the results between the collector shapes of the first (Figure 11a–d) and the second column (Figure 11f–i) should be understood as a consequence of the symmetry with respect to the NS axis of the studied configurations and of the symmetry with respect to this plane in the positions of the sun between the hours of the morning and afternoon.

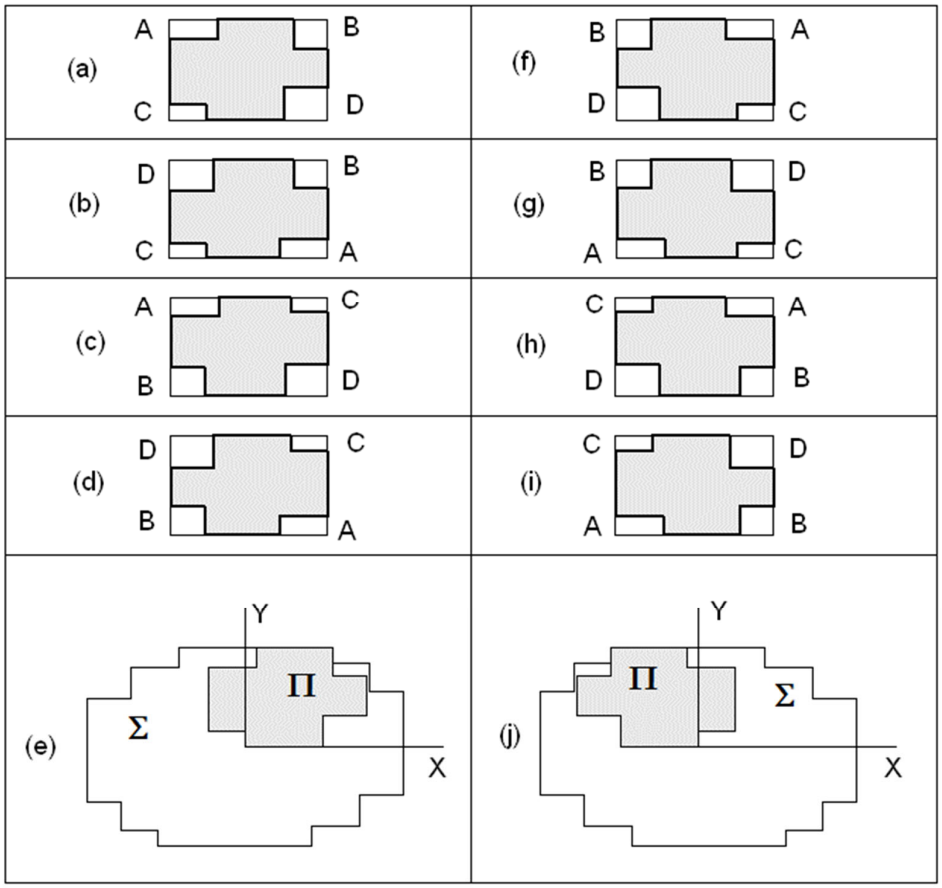

Figure 11. Set of collector shapes that generate identical annual incident radiation results. The forms (**a**–**d**) generate the same envelope Σ (**e**) and the set of symmetric figures with respect to a vertical axis (**f**–**i**) generate a symmetric envelope Σ′ of Σ (**j**).

The dependence of the values obtained with respect to the considered design variables was studied using an approximation and simplified model, in which the calculated annual radiation was expressed as a function of the following explanatory variables:

- Collector surface $S_{col}(m^2)$.
- Distance between trackers in east–west direction, D_{EW} (m)
- Distance between trackers in north–south direction, D_{NS} (m)
- Discriminatory variable of the type of configuration T (T = 1 for staggered configurations and T = 0 for regular grids).

In this sense, it is worth highlighting that the model described and used (for each of the 25,000 cases) can be considered a mathematical function of the variables proposed. However, the complexity of the model and the need to aggregate results on the different representative days made it difficult to know the weight or influence of each variable on the final results. Thus, to overcome this difficulty, this paper proposes to replace this complex function with a mathematical function of simple expression reproducing the result of the complex model with the least possible error. The reader should assume that this is not a statistical problem but rather a problem of adjustment or approximation of a simple expression function to a complex function, so that statistical methods are not applicable. To address the fit, the set of simple variables was extended with composite variables obtained as products and ratios of simple variables. The proposed function (29) was selected from the set of fits to linear functions of composite variables. It lacks a clear physical meaning, but it allows for reproduction of the results of the model with an average relative

error equal to 2.561 kWh/m²year; therefore, it is considered suitable for the study of the relative weight of the variables.

Equation (29) shows the mathematical expression of this model for which the parameters *a*, *b*, *c*, *d*, *e*, *f*, *g*, *h*, *l*, *r*, and *w* have been obtained by the least squares method (Table 3), with an adjustment coefficient $R^2 = 0.993$. Table 4 shows the synoptic values of the estimation errors of the model ε and ε_{rel}, given by Equations (30) and (31), where H_{year}^{est} is the annual solar irradiance on the solar collectors estimated according to Equation (28) and H_{year}^{adj} is the one approximated by the model (29). The low value obtained for the mean square error means that the equation can be considered valid for the study of dependence of the annual solar irradiance with respect to the variables S_{col}, D_{EW}, D_{NS}, and T.

$$H_{year}^{adj} = a + b\,S_{col} + c\,D_{EW} + \frac{d}{D_{EW}} + eD_{NS} + f\ {D_{NS}}^2 + g\,\frac{D_{EW}}{D_{NS}} + h\left(\frac{D_{EW}}{D_{NS}}\right)^2 + l\,\frac{S_{col}}{D_{NS}\,D_{EW}} + r\,\frac{D_{NS}\,D_{EW}}{S_{col}} + w\,T \quad (29)$$

$$\varepsilon = \left|H_{year}^{est} - H_{year}^{adj}\right| \quad (30)$$

$$\varepsilon_{rel} = \frac{\left|H_{year}^{est} - H_{year}^{adj}\right|}{H_{year}^{est}} \quad (31)$$

Table 3. Values obtained for the model of Equation (29).

Parameter	Units	Value
a	kWh/m² year	2656.366
b	kWh/m⁴ year	−0.960
c	kWh/m³ year	6.921
d	kWh/m year	−25.783
e	kWh/m³year	−756.012
f	kWh/m⁴ year	0.512
g	kWh/m² year	−167.750
h	kWh/m² year	19.071
l	kWh/m² year	−364.603
r	kWh/m² year	−1.365
w	kWh/m² year	−1.661

Table 4. Synoptics of the errors ε Equation (30) and ε_{rel} Equation (31) obtained for the model given by Equation (29).

	$\boldsymbol{\varepsilon}$ (kWh/m² year)	$\boldsymbol{\varepsilon_{rel}}$ (Dimensionless)
Number of cases	25000	25000
Average	3.302	$1.53 \cdot 10^{-3}$
Minimum	$4.67 \cdot 10^{-4}$	$2.099 \cdot 10^{-7}$
Maximum	35.913	$1.66 \cdot 10^{-2}$
Median	2.561	$1.15 \cdot 10^{-3}$

It is important to note that the model adjusted in Equation (30) does not consider the geometric shape of the collectors itself since, given that the mean error, $\bar{\varepsilon}$, of the proposed model is 3.3 kWh/m²year (Table 4), the geometric shape would not have an explanatory capacity superior to this $\bar{\varepsilon}$. This reasoning allowed us to conclude the little influence of the

shape of the collectors in facilities that follow the tracking/ back-tracking policy considered in this work.

For a better interpretation of the adjusted Equation (29), we can consider it as the addition of four terms separated by parentheses in Equation (32).

$$H_y^{adj} = a + \{b\, S_{col}\} + \left\{c\, D_{EW} + \frac{d}{D_{EW}} + eD_{NS} + f\ {D_{NS}}^2 + g\ \frac{D_{EW}}{D_{NS}} + h\left(\frac{D_{EW}}{D_{NS}}\right)^2\right\} + \left\{l\ \frac{S_{col}}{D_{NS}\, D_{EW}} + r\ \frac{D_{NS}\, D_{EW}}{S_{col}}\right\} + \{wT\} \quad (32)$$

The first term only depends on the collector surface S_{col}. Given that $b < 0$, it was found that, as the collectors were larger, the lower the annual incident radiation. This effect was due to the greater possibility of inter-shading as the collectors had more surface area. With the cases studied, the variation interval of the final result due exclusively to this term was 24 kWh/m² year.

The second term marks the importance of the geometric design of the plant given by D_{EW} and D_{NS}, regardless of whether it is a staggered or grid configuration. In the group of cases studied, the variation interval was 116 kWh/m² year.

The third term is interpreted as a function of the ground cover ratio (*GCR*) parameter defined by Equation (33).

$$GCR = \frac{S_{col}}{D_{NS}\, D_{EW}} \quad (33)$$

According to this definition, the third term considered in the model given by Equation (29) can be rewritten obtaining the expression (34). Thus, this term showed that the variation in this term was 104 kWh/m² year for the GCR values considered in the set of cases studied.

$$\left\{l\ \frac{S_{col}}{D_{NS}\, D_{EW}} + m\ \frac{D_{NS}\, D_{EW}}{S_{col}}\right\} = \left\{l\ GCR + \frac{m}{GCR}\right\} \quad (34)$$

Finally, given that the parameter w was negative, the term $\{wT\}$ implied a small difference of 1.6 kWh/m² year to the detriment of the installations that were arranged in a staggered pattern compared to those with a regular grid.

4. Conclusions

This work presents a novel methodology for the productive study of PV solar collectors mounted on dual-axis trackers. The study, applied to multiple cases, generated as variations with respect to the design adopted in an existing PV Plant ("El Molino", located in Córdoba) allows for identification of the design variables that fundamentally influence the annual incident irradiation on the solar collectors and, therefore, on the energy production of the PV plant. Specifically, by systematically varying the geometry of the collectors, the distance between them, and their spatial distribution, 25,000 case studies were simulated. For all of them, the annual incident solar radiation on the solar collectors was calculated, using for this the irradiance estimation model of Perez [43] and assuming that they were governed by a tracking strategy that optimized radiative capture while avoiding inter-shading between collectors [37,38]. Although a comprehensive methodology was used to study the case, it was difficult with the data set to understand the influence of each variable on the final result. Therefore, a simple function was fitted, which accurately reproduced the result of the complex model $\varepsilon\_rel = 0.00115$. From the irradiance data obtained for the different PV plant designs, a simple mathematical model has been obtained, Equation (29) with a high level of adjustment $(R^2 = 0.993)$ that represents the dependence of the annual solar irradiance on the PV plant with respect to design variables such as collector surface, S_{col}, NS and EW distances between collectors D_{NS} and D_{EW}, and spatial distribution of the collectors: regular or staggered grid. Thus, the proposed model

has made it possible to identify that the main variables that influence the annual incidence of irradiance are, in order of greatest influence, the geometric design of the plant as a function of the distances between its collectors, (D_{NS}, D_{EW}), the *GCR* of the installation and the surface of its collectors (S_{col}), which can lead to variations in the electrical production of the PV plant of up to 116 kWh/m²year, 104 kWh/m²year, and 24kWh/m²year. However, for practical purposes, with regard to the spatial distribution of the collectors, it is not appropriate to assume a better behaviour of the regular grid arrangement with respect to the staggered shape since the margin of 1.6 kWh/m²year for this variable falls within the uncertainty margin of the radiation prediction models. Similarly, the geometric shape of the collectors does not exert a significant influence on the irradiance received since it gives rise to variations of 3.3026 kWh/m²year , which, therefore, are lower than the uncertainty margin of the estimation model itself. Future works will study the influence of the shape in confluence with the orientation of the terrain.

Author Contributions: Conceptualization, F.J.G.-U., I.M.M.-G., and L.M.F.-A.; methodology, I.M.M.-G. and L.M.F.-A.; software, Á.P.-C.; validation, I.M.M.-G. and L.M.F.-A.; formal analysis, L.M.F.-A., I.M.M.-G., and F.J.G.-U.; bibliographic search, F.J.G.-U. and L.M.F.-A.; data curation, Á.P.-C.; writing—original draft preparation, L.M.F.-A., F.J.G.-U., and I.M.M.-G.; writing—review and editing, F.J.G.-U., I.M.M.-G., and L.M.F.-A.; supervision, I.M.M.-G. and L.M.F.-A. All authors have read and agreed to the published version of the manuscript.

Funding: This research is partially supported by the CLARA Project, which has received funding from the European Union's Horizon 2020 research and innovation programme under Grant Agreement No 730482.

Acknowledgments: Authors appreciate the support of Professor Rafael López-Luque.

Conflicts of Interest: The authors declare no conflict of interest.

Abbreviations

A_0	reference collector surface
A_i	generic collector surface
D_{EW}	distance between trackers in east–west direction
d_i	geometric displacement vector from polygon Π_0 to Π'_i
d_n	Julian day
D_{NS}	distance between trackers in north–south direction
d_{Xi}	X component of d_i
d_{Yi}	Y component of d_i
F_1, F_2	weighting factors for the decomposition of the inclined diffuse radiation
GCR	ground cover ratio
H_m	incident radiation on the collectors on each representative day of a month according to Klein
H_{year}	annual global radiation
H_{year}^{est}	annual solar irradiance on the solar collectors estimated according to Equation (28)
H_{year}^{adj}	annual solar irradiance on the solar collectors estimated according to Equation (29)
$\vec{\imath}, \vec{\jmath}, \vec{k}$	unit vectors associated to a local Cartesian system
I	global solar irradiance on the tilted collector
I_B	direct solar irradiance on horizontal plane
I_D	diffuse solar irradiance
L_x	horizontal longitude of the collector before cuts
L_y	vertical longitude of the collector before cuts
$\vec{n}$	normal vector to the surface
N_D	different design of the inter-distances between collectors

N_G	different forms of collector shape
N_m	number of days in the month m
N_S	possible spatial distributions of the solar trackers in the plant
N_T	different combinations of geometric designs result of crossing $N_G \cdot N_D \cdot N_S$
P_0	position of the reference collector
P_i	position of a generic collector
$\vec{s}$	solar vector
S_{col}	collector surface
s_x, s_y, s_z	components of solar vector
T	discriminatory variable of the type of configuration
X_{dl}	x-coordinate of the vertex corresponding to the cut made in the lower left corner
X_{dr}	x-coordinate of the vertex corresponding to the cut made in the lower right corner
X_{env}	array with the x-coordinates of the collector shape
X_{ul}	x-coordinate of the vertex corresponding to the cut made in the upper left corner
X_{ur}	x-coordinate of the vertex corresponding to the cut made in the upper right corner
Y_{dl}	y-coordinate of the vertex corresponding to the cut made in the lower left corner
Y_{dr}	y-coordinate of the vertex corresponding to the cut made in the lower right corner
Y_{env}	array with the y-coordinates of the collector shape
Y_{ul}	y-coordinate of the vertex corresponding to the cut made in the upper left corner
Y_{ur}	y-coordinate of the vertex corresponding to the cut made in the upper right corner
$\vec{u}$	horizontal vector to the maximum slop direction of the collector plane
v	parallel vector to the maximum slop direction of the collector plane

Greek Letters

β	inclination angle of the terrain
γ	azimuth angle of the collector rotation axis
δ	solar declination
ε	estimation error of the proposed model
ε_{rel}	relative error of the proposed model
θ	angle of incidence of sunbeams on the inclined plane
θ_z	solar zenith angle
ρ	albedo
φ	latitude
Ω	Earth's rotation speed
Γ	daily angle
Π_0	reference polygon collector
Π_i	generic polygon collector
Π'_i	projection of generic polygon collector over ψ
ψ	plane that contains the reference collector Π_0

Appendix A. Demonstration of the Dicotomic Criterion for Determining the Inter-shading between Solar Collectors

To determine if there is inter-shading between collectors, in this work, a dichotomous criterion is used, based on Minkowski's algebra [44–46], according to which there is inter-

shading between two collectors Π_0 y Π_i if and only if the displacement vector $\vec{d}_i$ from collector Π_0 to Π'_i, which is the projection of collector Π_i on the plane ψ that contains Π_0 and can be considered a translation of Π_0, is included within the plane curve Σ, which is obtained as the envelope of the family of all polygons that can be drawn in the plane ψ when translating the polygon Π_0, with the condition that its perimeter is in contact with the origin of the reference system contained in ψ.

Thus, this appendix demonstrates this dichotomous criterion for two generic surfaces: Π and its translation Π_T.

"A polygon $\boldsymbol{\Pi}$ and its translation $\boldsymbol{\Pi_T}$ intersect if and only if the translation vector $\boldsymbol{\overrightarrow{OP}}$ of $\boldsymbol{\Pi_T}$ with respect to $\boldsymbol{\Pi}$ is included in the envelope $\boldsymbol{\Sigma}$".

The demonstration has two steps:

- Step 1: If $\overrightarrow{OP}$ is included in Σ, Π and Π_T intersect.

Since $\overrightarrow{OP}$ is included in Σ (Figure A1a), there will be at least one polygon Π that, passing through the origin of coordinates O, encloses point P (Figure A1b). If this polygon is translated following $\overrightarrow{OP}$, it is evident that point O is translated to P (Figure A1c). Since this point P, the boundary of Π_T, is interior to Π, there will be an intersection between Π and Π_T.

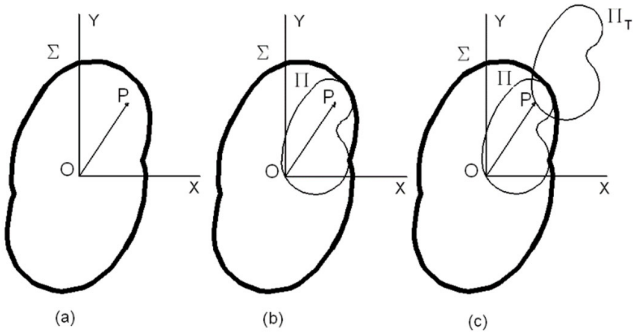

Figure A1. Demonstration sequence: If $\overrightarrow{OP}$ is included in Σ, Π and Π_T intersect.

- Step 2: If Π and Π_T intersect, $\overrightarrow{OP}$ is included in Σ.

If Π and Π_T intersect, there will exist, at least. a point *P*, of the perimeter of Π_T that is included in Π. By calling *O* the origin of *P*, it is possible to define the vector $\overrightarrow{OP}$ (Figure A2a). If the system of coordinate axes passing through O is considered and the envelope Σ is drawn, it is evident that the point *P* is included in Σ (Figure A2b).

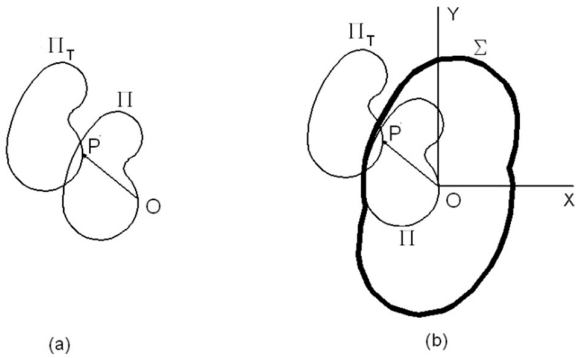

Figure A2. Demonstration sequence: If Π and Π_T intersect, $\overrightarrow{OP}$ is included in Σ.

Appendix B. Obtaining the Generic Form σ for Collectors with Cuts

In this appendix, the procedure for obtaining the flat curve Σ associated with a collecting surface Π with a generic shape is explained in detail so that it is valid for all the collector shapes considered in this work.

Letting a plane ψ and a reference system OXY be in this plane, we considered a polygon Π contained in ψ with the shape of a rectangle with sides L_x and L_y with the vertices trimmed, the coordinates of these vertices being: (X_{ul}, Y_{ul}), (X_{ur}, Y_{ur}), (X_{dl}, Y_{dl}), and (X_{dr}, Y_{dr}) (Figure A3).

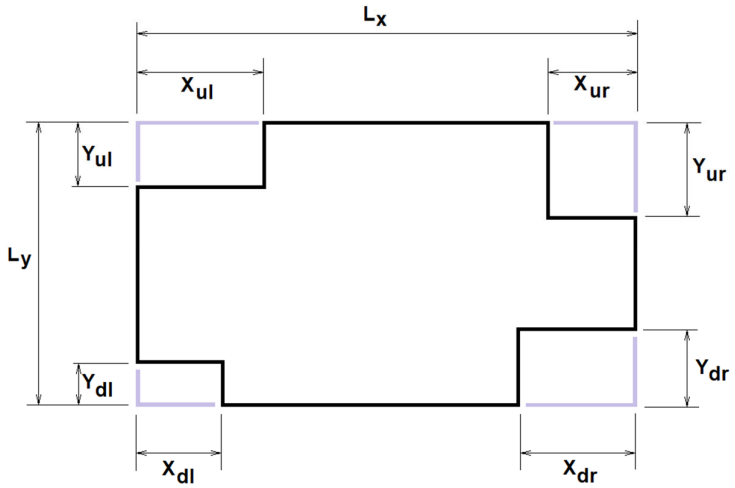

Figure A3. Representation of the generic collector surface Π based on a rectangle with sides L_X and L_Y with the vertices cut off.

The analysis of all the translations allows us to obtain the coordinates of the perimeter of Σ. In general, Σ is a polygon with 28 vertices that depend on the dimensions reflected in Figure A3 according to expression (A1).

$$\Sigma = \Sigma(L_x, L_y, X_{ul}, Y_{ul}, X_{ur}, Y_{ur}, X_{dl}, Y_{dl}, X_{dr}, Y_{dr}) \quad \text{(A1)}$$

In this way, these coordinates can be structured in two arrays of 28 elements: Xenv (28) and Yenv (28). Next, the VBA programming code that allows obtaining each of these coordinates is shown.

```
Xenv(1) = Lx − Xur − Xdl: Yenv(1) = Ly
If Yur<Ydl Then
Xenv(2) = Xenv(1): Yenv(2) = Yenv(1) − Yur
Xenv(3) = Xenv(1) + Xur: Yenv(3) = Yenv(1) − Yur
Else
Xenv(2) = Xenv(1): Yenv(2) = Yenv(1) − Ydl
Xenv(3) = Xenv(1) + Xdl: Yenv(3) = Yenv(1) − Ydl
End If

Xenv(7) = Lx: Yenv(7) = Ly − Yur − Ydl
If Xur<Xdl Then
Xenv(6) = Xenv(7) − Xur: Yenv(6) = Yenv(7)
Xenv(5) = Xenv(7) − Xur: Yenv(5) = Yenv(7) + Yur
Else
Xenv(6) = Xenv(7) − Xdl: Yenv(6) = Yenv(7)
Xenv(5) = Xenv(7) − Xdl: Yenv(5) = Yenv(7) + Ydl
End If
Xenv(4) = Xenv(3): Yenv(4) = Yenv(5)

Xenv(11) = Lx: Yenv(11) = -Ly + Ydr + Yul
```

```
If Xdr<Xul Then
Xenv(11) = Xenv(11) − Xdr: Yenv(11) = Yenv(11)
Xenv(10) = Xenv(11) − Xdr: Yenv(10) = Yenv(11) − Ydr
Else
Xenv(11) = Xenv(11) − Xul: Yenv(11) = Yenv(11)
Xenv(10) = Xenv(11) − Xul: Yenv(10) = Yenv(11) − Yul
End If
Xenv(11) = Xenv(12): Yenv(11) = Yenv(10)

Xenv(14) = Lx − Xdr − Xul: Yenv(14) = -Ly
If Ydr<Yul Then
Xenv(13) = Xenv(14): Yenv(13) = Yenv(14) + Ydr
Xenv(12) = Xenv(14) + Xdr: Yenv(12) = Yenv(14) + Ydr
Else
Xenv(13) = Xenv(14): Yenv(13) = Yenv(14) + Yul
Xenv(12) = Xenv(14) + Xul: Yenv(12) = Yenv(14) + Yul
End If

For i = 15 To 211
Xenv(i) = -Xenv(i − 14)
Yenv(i) = -Yenv(i − 14)
Next i
```

However, when there is some kind of symmetry or when any of the dimensions of the cutouts is null, some coordinates contained in the Xenv () and Yenv () arrays will be repeated. In these cases, the number of vertices of Σ will be less than 28. After eliminating the possible repeated points, it is mathematically verified that there are four combinations or symmetries that generate the same polygon Σ Equation (A2).

$$\begin{aligned}&\Sigma\left(L_x, L_y, X_{ul}, Y_{ul}, X_{ur}, Y_{ur}, X_{dl}, Y_{dl}, X_{dr}, Y_{dr}\right) =\\ &\Sigma\left(L_x, L_y, X_{dr}, Y_{dr}, X_{ur}, Y_{ur}, X_{dl}, Y_{dl}, X_{ul}, Y_{ul}\right) =\\ &\Sigma\left(L_x, L_y, X_{ul}, Y_{ul}, X_{dl}, Y_{dl}, X_{ur}, Y_{ur}, X_{dr}, Y_{dr}\right) =\\ &\Sigma\left(L_x, L_y, X_{dr}, Y_{dr}, X_{ur}, Y_{ur}, X_{dl}, Y_{dl}, X_{ul}, Y_{ul}\right)\end{aligned} \quad \text{(A2)}$$

In this way, it is possible to obtain the envelope Σ to the family of polygons Π on which the dichotomous criterion of inter-shading between collectors will be based.

References

1. López, I.; Arriaga, A.; Pardo, M. La dimensión social del concepto de desarrollo sostenible: ¿La eterna Olvidada? *Rev. Span. Sociol.* **2018**, *27*, doi:10.22325/fes/res.2018.2.
2. International Energy Agency (IEA). *Renewables 2020*; IEA: Paris, France, 2020.
3. Andre, T.; Guerra, F. *Renewables Global Status Report*; REN21: Paris, France, 2020; ISBN 978-3-948393-00-7
4. Kannan, N.; Vakeesan, D. Solar energy for future world: A review. *Renew. Sustain. Energy Rev.* **2016**, *62*, 1092–1105.
5. Eldin, S.A.S.A.S.; Abd-Elhady, M.S.S.; Kandil, H.A.A. Feasibility of solar tracking systems for PV panels in hot and cold regions. *Renew. Energy* **2016**, *85*, 228–233.
6. Salas, V.; Olias, E. Overview of the photovoltaic technology status and perspective in Spain. *Renew. Sustain. Energy Rev.* **2009**, *13*, 1049–1057.
7. Singh, R.; Kumar, S.; Gehlot, A.; Pachauri, R. An imperative role of sun trackers in photovoltaic technology: A review. *Renew. Sustain. Energy Rev.* **2018**, *82*, 3263–3278.
8. AL-Rousan, N.; Isa, N.A.M.; Desa, M.K.M. Advances in solar photovoltaic tracking systems: A review. *Renew. Sustain. Energy Rev.* **2018**, *82*, 2548–2569.
9. Frydrychowicz-Jastrzębska, G.; Bugała, A. Modeling the Distribution of Solar Radiation on a Two-Axis Tracking Plane for Photovoltaic Conversion. *Energies* **2015**, *8*, 1025–1041.
10. Hafez, A.Z.; Yousef, A.M.; Harag, N.M. Solar tracking systems: Technologies and trackers drive types—A review. *Renew. Sustain. Energy Rev.* **2018**, *91*, 754–782.
11. Lee, C.-Y.; Chou, P.-C.; Chiang, C.-M.; Lin, C.-F. Sun Tracking Systems: A Review. *Sensors* **2009**, *9*, 3875–3890.
12. Antonanzas, J.; Urraca, R.; Martinez-de-Pison, F.J.; Antonanzas, F. Optimal solar tracking strategy to increase irradiance in the plane of array under cloudy conditions: A study across Europe. *Sol. Energy* **2018**, *163*, 122–130.
13. Bahrami, A.; Okoye, C.O. The performance and ranking pattern of PV systems incorporated with solar trackers in the northern hemisphere. *Renew. Sustain. Energy Rev.* **2018**, *97*, 138–151.

14. Quesada, G.; Guillon, L.; Rousse, D.R.; Mehrtash, M.; Dutil, Y.; Paradis, P.-L. Tracking strategy for photovoltaic solar systems in high latitudes. *Energy Convers. Manag.* **2015**, *103*, 147–156.
15. Hammad, B.; Al-Sardeah, A.; Al-Abed, M.; Nijmeh, S.; Al-Ghandoor, A. Performance and economic comparison of fixed and tracking photovoltaic systems in Jordan. *Renew. Sustain. Energy Rev.* **2017**, *80*, 827–839.
16. Talavera, D.L.; Muñoz-Cerón, E.; Ferrer-Rodríguez, J.P.; Pérez-Higueras, P.J. Assessment of cost-competitiveness and profitability of fixed and tracking photovoltaic systems: The case of five specific sites. *Renew. Energy* **2019**, *134*, 902–913.
17. Hua, Z.; Ma, C.; Lian, J.; Pang, X.; Yang, W. Optimal capacity allocation of multiple solar trackers and storage capacity for utility-scale photovoltaic plants considering output characteristics and complementary demand. *Appl. Energy* **2019**, *238*, 721–733.
18. Ali Jallal, M.; Chabaa, S.; Zeroual, A. A novel deep neural network based on randomly occurring distributed delayed PSO algorithm for monitoring the energy produced by four dual-axis solar trackers. *Renew. Energy* **2020**, *149*, 1182–1196.
19. Eke, R.; Senturk, A. Performance comparison of a double-axis sun tracking versus fixed PV system. *Sol. Energy* **2012**, *86*, 2665–2672.
20. Şenpinar, A.; Cebeci, M. Evaluation of power output for fixed and two-axis tracking PVarrays. *Appl. Energy* **2012**, *92*, 677–685.
21. Bahrami, A.; Okoye, C.O.; Atikol, U. The effect of latitude on the performance of different solar trackers in Europe and Africa. *Appl. Energy* **2016**, *177*, 896–906.
22. Koussa, M.; Cheknane, A.; Hadji, S.; Haddadi, M.; Noureddine, S. Measured and modelled improvement in solar energy yield from flat plate photovoltaic systems utilizing different tracking systems and under a range of environmental conditions. *Appl. Energy* **2011**, *88*, 1756–1771.
23. Seme, S.; Štumberger, G.; Voršič, J. Maximum efficiency trajectories of a two-axis sun tracking system determined considering tracking system consumption. *IEEE Trans. Power Electron.* **2011**, *26*, 1280–1290.
24. Gómez-Uceda, F.J.; Ramirez-Faz, J.; Varo-Martinez, M.; Fernández-Ahumada, L.M. New Omnidirectional Sensor Based on Open-Source Software and Hardware for Tracking and Backtracking of Dual-Axis Solar Trackers in Photovoltaic Plants. *Sensors* **2021**, *21*, 726.
25. Fernández-Ahumada, L.M.; Ramírez-Faz, J.; López-Luque, R.; Varo-Martínez, M.; Moreno-García, I.M.; Casares de la Torre, F. Influence of the design variables of photovoltaic plants with two-axis solar tracking on the optimization of the tracking and backtracking trajectory. *Sol. Energy* **2020**, *208*, 89–100.
26. Lorenzo, E.; Pérez, M.; Ezpeleta, A.; Acedo, J. Design of tracking photovoltaic systems with a single vertical axis. *Prog. Photovolt. Res. Appl.* **2002**, *10*, 533–543.
27. Karatepe, E.; Boztepe, M.; Çolak, M. Development of a suitable model for characterizing photovoltaic arrays with shaded solar cells. *Sol. Energy* **2007**, *81*, 977–992.
28. Kaushika, N.D.; Gautam, N.K. Energy yield simulations of interconnected solar PV arrays. *IEEE Trans. Energy Convers.* **2003**, *18*, 127–134.
29. Woyte, A.; Nijs, J.; Belmans, R. Partial shadowing of photovoltaic arrays with different system configurations: Literature review and field test results. *Sol. Energy* **2003**, *74*, 217–233.
30. Trzmiel, G.; Głuchy, D.; Kurz, D. The impact of shading on the exploitation of photovoltaic installations. *Renew. Energy* **2020**, *153*, 480–498.
31. Díaz-Dorado, E.; Suárez-García, A.; Carrillo, C.J.; Cidrás, J. Optimal distribution for photovoltaic solar trackers to minimize power losses caused by shadows. *Renew. Energy* **2011**, *36*, 1826–1835.
32. Martínez-Moreno, F.; Muñoz, J.; Lorenzo, E. Experimental model to estimate shading losses on PV arrays. *Sol. Energy Mater. Sol. Cells* **2010**, *94*, 2298–2303.
33. Perpiñán, O. Cost of energy and mutual shadows in a two-axis tracking PV system. *Renew. Energy* **2012**, *43*, 331–342.
34. Narvarte, L.; Lorenzo, E. Tracking and ground cover ratio. *Prog. Photovolt. Res. Appl.* **2008**, *16*, 703–714.
35. Panico, D.; Garvison, P.; Wenger, H.; Shugar, D. Backtracking: A novel strategy for tracking PV systems. In Proceedings of the Conference Record of the Twenty-Second IEEE Photovoltaic Specialists Conference 1991, Las Vegas, NV, USA, 7–11 October 1991; pp. 668–673.
36. DEGERiberica. Referencias. Available online: https://degeriberica.com/referencias/ (accessed on 20 January 2021).
37. Fernández-Ahumada, L.M.; Casares, F.J.; Ramírez-Faz, J.; López-Luque, R. Mathematical study of the movement of solar tracking systems based on rational models. *Sol. Energy* **2017**, *150*, 20–29.
38. Fernández-Ahumada, L.M.; Ramírez-Faz, J.; López-Luque, R.; Varo-Martínez, M.; Moreno-García, I.M.; Casares de la Torre, F. A novel backtracking approach for two-axis solar PV tracking plants. *Renew. Energy* **2020**, *145*, 1214–1221.
39. Braun, J.E.; Mitchell, J.C. Solar geometry for fixed and tracking surfaces. *Sol. Energy* **1983**, *31*, 439–444.
40. Reda, I.; Andreas, A. Solar position algorithm for solar radiation applications. *Sol. Energy* **2004**, *76*, 577–589.
41. Riley, D.; Hansen, C. Sun-Relative Pointing for Dual-Axis Solar Trackers Employing Azimuth and Elevation Rotations. *J. Sol. Energy Eng.* **2015**, *137*, 031008, doi:10.1115/1.4029379.
42. Kelly, N.A.; Gibson, T.L. Improved photovoltaic energy output for cloudy conditions with a solar tracking system. *Sol. Energy* **2009**, *83*, 2092–2102.
43. Perez, R.; Ineichen, P.; Seals, R.; Michalsky, J.; Stewart, R. Modeling daylight availability and irradiance components from direct and global irradiance. *Sol. Energy* **1990**, *44*, 271–289.
44. Avnaim, F.; Boissonnat, J.-D. Polygon placement under translation and rotation. *RAIRO Theor. Inform. Appl.* **1989**, *23*, 5–28.
45. Chazelle, B. The polygon containment problem. *Adv. Comput. Res.* **1983**, *1*, 1–33.
46. Lozano-Pérez, T. Spatial Planning: A Configuration Space Approach. *IEEE Trans. Comput.* **1983**, doi:10.1109/TC.1983.1676196.

47. Klein, S.A. Calculation of monthly average insolation on tilted surfaces. *Sol. Energy* **1977**, *19*, 325–329.
48. Posadillo, R.; López Luque, R. A sizing method for stand-alone PV installations with variable demand. *Renew. Energy* **2008**, *33*, 1049–1055.